Fibers and Polymers
https://doi.org/10.1007/s12221-025-01285-5

Online ISSN 1875-0052
Print ISSN 1229-9197

REGULAR ARTICLE

Support Vector Regression Prediction of Dye Saturation in Recycled PET/PCT Microfibers for Deep Black Shade

Hyeokjun Cho[1] · Jae Wang Ko[2] · Seung Geol Lee[1,3]

Received: 2 September 2025 / Revised: 17 November 2025 / Accepted: 5 December 2025

Abstract

The textile dyeing industry faces increasing pressure to reduce chemical usage and improve resource efficiency. This study applies Support Vector Regression (SVR) to predict the dye saturation region of recycled PET/PCT fabrics dyed with a single disperse black dye. The objective is to identify the optimal dye concentration range using a machine learning–based approach. K/S values obtained from fabrics dyed at various concentrations were used to train and evaluate SVR models. Model performance was assessed using standard regression metrics such as coefficient of determination (R^2), mean absolute error (MAE), and mean squared error (MSE). The SVR model demonstrated high predictive accuracy and effectively captured gradient transitions near the saturation region. From the predicted K/S curves, the point at which further dye addition yields no significant increase in color strength was quantitatively determined. Despite the limited number of training samples, the model successfully learned the nonlinear characteristics of the dyeing response and showed greater robustness to outliers than conventional regression methods. These findings support the potential of SVR as a reliable tool for predicting dye saturation points and optimizing dye use in deep black shade development, contributing to reduced experimental workload and improved resource efficiency.

Keywords Recycled PET · PCT · Deep black shade · Machine learning · Support vector regression

1 Introduction

Conventional textile dyeing requires substantial amounts of both resources and water, which results in the generation of large volumes of polluted wastewater [1–7]. This effluent often contains toxic substances such as heavy metals (for example, chromium and lead) and azo compounds that are difficult to eliminate [8–13]. Advanced treatment processes are required to remove these pollutants, but such methods demand additional energy and chemicals, significantly increasing treatment costs [14, 15]. Additionally, the high dyeing temperatures and multiple washing cycles contribute to substantial energy consumption and carbon emissions. Therefore, textile dyeing is recognized as a major contributor to environmental pollution and greenhouse gas emissions, which highlights the urgent need for more sustainable practices.

To address these challenges, researchers are exploring material–based solutions in addition to improvements in wastewater treatment technologies [16–22]. One promising approach involves using recycled polyester (rPET) blended with polycyclohexylenedimethylene terephthalate (PCT), a high–performance copolyester that has a lower carbon footprint. This study specifically employs an environmentally friendly microfiber suede fabric made from a blend of rPET and PCT fibers, which combines recycled content with excellent dyeability. The rPET component promotes resource circularity by reusing plastic waste, and PCT contributes superior heat resistance and dimensional stability that improve color stability and dye affinity during dyeing [23, 24]. Moreover, the fabric's fine microfiber structure increases the surface area available for dye diffusion, which enables deep and uniform black coloration [25, 26]. These

✉ Seung Geol Lee
seunggeol.lee@unist.ac.kr

[1] Department of Materials Science and Engineering, Ulsan National Institute of Science and Technology (UNIST), Ulsan 44919, Republic of Korea

[2] Korea Institute of Materials Convergence Technology (KIMCO), Busan 47154, Republic of Korea

[3] Graduate School of Semiconductor Materials and Devices Engineering, Ulsan National Institute of Science and Technology (UNIST), Ulsan 44919, Republic of Korea

Published online: 20 December 2025

characteristics enhance dye uptake efficiency and can reduce the energy required compared to conventional polyester dyeing. Consequently, the rPET/PCT fabric offers a promising foundation for dyeing processes that aim to achieve both high performance and environmental sustainability.

This study aims to quantitatively analyze the saturation behavior observed in the dyeing process using disperse dyes on the aforementioned fabric. As the dye concentration increases during dyeing, the apparent color strength (K/S) initially rises sharply, but beyond a certain point, the rate of increase slows as the fiber approaches its maximum dye absorption capacity [27, 28]. The point at which no further meaningful increase in color strength is observed is referred to as the dye saturation point. Accurately identifying this point is essential for minimizing unnecessary dye consumption and reducing wastewater discharge.

When dye is added beyond the saturation point, the excess dye that is not absorbed by the fiber tends to remain in the solution and is likely to be discharged as wastewater. This not only results in resource waste but also contributes to environmental pollution [29–32]. On the other hand, insufficient dye concentration can lead to challenges in reaching the target color intensity and may result in poor color uniformity across the fabric. Therefore, accurately predicting the optimal dye concentration based on the type and structure of the fiber is essential for ensuring both quality consistency and cost–effectiveness in the dyeing process. However, conventional approaches to optimizing dyeing conditions rely on repetitive and time–consuming experiments involving manual adjustments of process parameters, which require substantial cost and resources [33–36].

Consequently, machine learning–based prediction techniques have gained increasing attention as practical tools for optimizing textile dyeing processes [37–42]. Machine learning algorithms can learn complex nonlinear relationships from experimental data. This capability enables rapid prediction of dyeing outcomes under new conditions. In this study, we adopted Support Vector Regression (SVR) to quantitatively model the nonlinear relationship between dye concentration and K/S. SVR was chosen for its ability to achieve high accuracy with limited data by mapping inputs into a higher–dimensional feature space via kernel functions [43–46]. It has also demonstrated robust generalization with minimal overfitting, even for resource–intensive processes like textile dyeing [47, 48]. We evaluated the SVR model's performance in capturing the saturation curve and compared it with several other regression algorithms to validate its reliability.

By predicting the dye saturation point using SVR, we aim to enhance color performance while reducing the use of resources. This data–driven approach decreases dependence on traditional trial–and–error methods, which in turn can significantly lower dye, water, and energy consumption [49, 50]. Furthermore, the SVR model can be adapted to specific fiber blends, such as the rPET/PCT combination, by incorporating fiber–specific characteristics into the training dataset. This customization enables a shift from empirical process optimization to a more systematic and efficient data–driven methodology. As a result, this strategy has the potential to deliver meaningful reductions in resource use, production costs, and environmental impact, all of which are critical objectives in sustainable textile dyeing. The framework proposed in this study is also expected to be applicable to other composite fiber systems, thereby supporting the broader implementation of environmentally responsible dyeing practices throughout the textile industry.

2 Experimental

2.1 Materials

In this study, a black dope–dyed microfiber suede fabric provided by Huvis Co., Ltd. was used as the dyeing specimen. The fabric is a composite material composed of 50% recycled PET fibers and 50% PCT fibers, impregnated with approximately 30% polyurethane (PU) resin. The main characteristics of the fabric used for dyeing are summarized in Fig. 1. Recycled PET is a fiber regenerated from waste PET materials through mechanical or chemical recycling

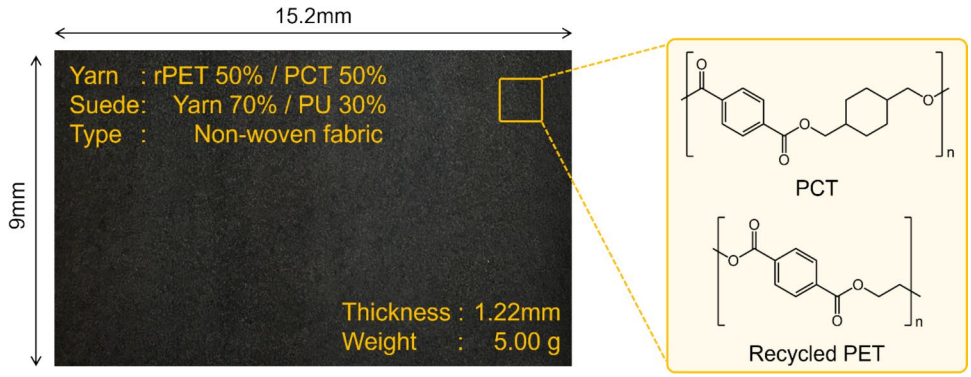

Fig. 1 Characterization of the rPET/PCT microfiber suede fabric

processes. PCT is a copolyester synthesized via esterification polymerization of terephthalic acid (TPA) or dimethyl terephthalate (DMT) with the precursor 1,4–cyclohexanedimethanol (CHDM). The dyeing process employed Synolon Black AK–NB, an anthraquinone–based disperse dye (KISCO Co., Ltd., Korea), and acetic acid (CH_3COOH, SAMIL Co., Ltd., Korea) was added to adjust the pH. For dye dispersion, Sunsolt RM–340S (NICCA KOREA Co., Ltd., Japan) was used as the dispersing agent. In the subsequent reduction cleaning step, a reducing solution was prepared using a combination of Sera Con M–FAS (DyStar, Singapore) and sodium hydroxide (NaOH, SAMIL Co., Ltd., Korea).

2.2 Dyeing and Reduction Cleaning

Dyeing was carried out under high–temperature and high–pressure conditions using an infrared dyeing machine (DL–6000, Daelim Starlet Co., Korea). The liquor ratio was set to 1:20 with a fabric weight of 5 g, and the dye concentration was varied from 0.1 to 4.5% on the weight of fabric (owf) in increments of 0.1%. The pH of the dye bath was adjusted to 4.8 by adding CH_3COOH, and 0.7 mL of dispersing agent was added to ensure stable dispersion of the dye. Dyeing was performed by combining temperature conditions ranging from 100 °C to 130 °C with dyeing times between 10 and 60 min. Among these conditions, 110 °C for 40 min yielded the best dyeing performance and was therefore selected as the optimal dyeing condition. The changes in the L* value, which represents the brightness of the fabric, and the K/S value under different dyeing conditions are illustrated in Fig. 2(a). Figure 2(b) schematically presents the final optimized dyeing conditions and the subsequent reduction cleaning process. After dyeing, reduction cleaning was carried out to remove unfixed residual dye from the fabric surface. A reducing solution was prepared using 6 g/L of reducing agent and 6 mL/L of NaOH at a liquor ratio of 1:20, and the fabric was treated at 80 °C for 20 min. After the reduction cleaning, the fabric was rinsed with warm water and then dried to obtain the final dyed specimen.

2.3 Color Measurement

To evaluate the dyeing properties of the dyed fabric, surface reflectance was measured using a spectrophotometer (SCINCO Co., Ltd., Korea) under standard conditions of 10° observer angle and D65 light source. Measurements were taken in the visible wavelength range of 360 to 740 nm at 20 nm intervals. Based on these data, the L* value and the surface reflectance at the maximum absorption wavelength were obtained. The K/S value was calculated using Eq. (1):

$$K/S = \frac{(1-R)^2}{2R} \tag{1}$$

where K is the absorption coefficient, S is the scattering coefficient, and R represents the reflectance. To minimize

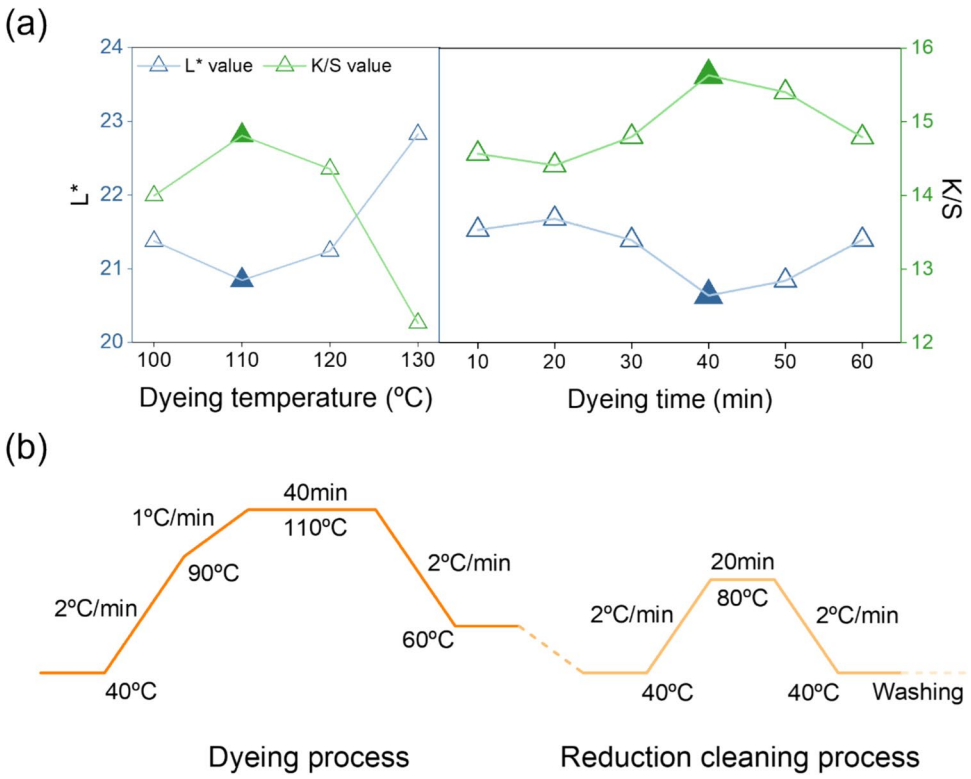

Fig. 2 **a** L* and K/S values measured under various dyeing temperatures (100–130 °C) and times (10–60 min), **b** dyeing and reduction cleaning processes applying the optimal dyeing temperature (110 °C) and time (40 min)

measurement error, each fabric sample was measured four times, and the average value was used for analysis.

2.4 Dataset and Modeling Setup

In this study, a total of 45 color data points were obtained by dyeing fabric samples with dye concentrations ranging from 0.1–4.5% owf in 0.1% increments. The dye concentration used for each sample was set as the input variable, and the corresponding K/S value was used as the output variable. All data were quantitatively obtained through experimental measurements. The dataset was designed to enable precise learning of the color strength curve across the full dye concentration range (0.1–4.5% owf) and to accurately capture the dye saturation region. While conventional regression analysis typically involves dividing the data into training and validation sets to assess the generalization performance of the model, the primary objective of this study was not merely to achieve numerical prediction accuracy but to quantitatively identify the gradient changes in the curve and the location of the saturation region. In particular, the saturation point corresponds to only a specific section within the overall concentration range. If data from this region are excluded for validation, the model may fail to learn the critical area it is intended to predict. Moreover, given the limited number of available data points, setting aside a portion for validation may reduce the sensitivity and reliability of the saturation point prediction. Therefore, the entire dataset was used for model training to ensure the model learned the full curve from the initial increase and peak point to the gradual changes in the saturation region. Instead of a conventional train–test split, the model's extrapolation accuracy was verified by comparing its predictions with additional dyeing experiments conducted beyond the training concentration range. The entire data processing and predictive model development were carried out using Python version 3.10.0. Scikit–learn version 1.6.1 was employed for model training, and data input, output, and computations were performed using packages including Pandas and NumPy.

3 Results and Discussion

3.1 Model Comparison

Various regression models were compared to predict the K/S values according to dye concentration. The performance of each model was evaluated based on mean absolute error (MAE), mean squared error (MSE), and coefficient of determination (R^2). MAE represents the average of the absolute differences between predicted and actual values. Since its unit is the same as that of the output variable, it allows for intuitive interpretation and provides a quantitative measure of the overall prediction error. On the other hand, MSE is calculated by averaging the squared errors, making it more sensitive to large deviations. This characteristic makes MSE a useful metric for evaluating a model's sensitivity to outliers and comparing its robustness [51, 52]. The formulas for MAE and MSE are presented in Eqs. (2) and (3), respectively.

$$MAE = \frac{1}{n}\sum_{i=1}^{n}|y_i - \hat{y}_i| \tag{2}$$

$$MSE = \frac{1}{n}\sum_{i=1}^{n}(y_i - \hat{y}_i)^2 \tag{3}$$

where, y_i denotes the experimentally observed value, and $\hat{y}_i$ represents the value predicted by the model. The R^2 value indicates the proportion of the total variance in the data that is explained by the model, and it quantitatively evaluates the correlation between the predicted and actual values. The R^2 value ranges from 0 to 1, with values closer to 1 indicating that the model explains the actual data more effectively. Mathematically, it is defined as the ratio of the explained sum of squares (ESS) to the total sum of squares (TSS), and is commonly expressed as one minus the ratio of the residual sum of squares (RSS) to the total sum of squares. However, R^2 alone indicates only how well the model fits the training data; a high R^2 does not guarantee strong predictive ability [53, 54]. In the case of high–dimensional problems or models prone to overfitting, a high R^2 value may suggest inflated model performance. Thus, it was interpreted alongside error indicators such as MAE and MSE. The definition of R^2 is given in Eq. (4).

$$R^2 = \frac{ESS}{TSS} = 1 - \frac{RSS}{TSS} = 1 - \frac{\sum_{i=1}^{n}(y_i - \hat{y}_i)^2}{\sum_{i=1}^{n}(y_i - \overline{y}_i)^2} \tag{4}$$

where, $\overline{y}$ denotes the mean of the experimentally observed values. To identify the model with the best performance, a total of 8 models were evaluated: Decision Tree (DT), SVR, Artificial Neural Network (ANN), Ridge Regression, Linear Regression, Support Vector Machine (SVM), Polynomial Regression, and Random Forest (RF). Figure 3 presents the predicted K/S values obtained from each regression model for dye concentrations ranging from 0.1–4.5% owf, along with the actual K/S values and the corresponding R^2, MAE, and MSE values for each model.

The evaluation results in Fig. 3(j) and 3(k) show that the SVR model achieved the lowest error and the highest R^2 among all models, with an MAE of 0.2959, MSE of 0.1579, and R^2 of 0.9588. In addition, the residual analysis in Fig. S1 confirmed the reliability of the SVR model, which showed the smallest standard deviation of residuals (0.3938), further supporting its stable fitting performance

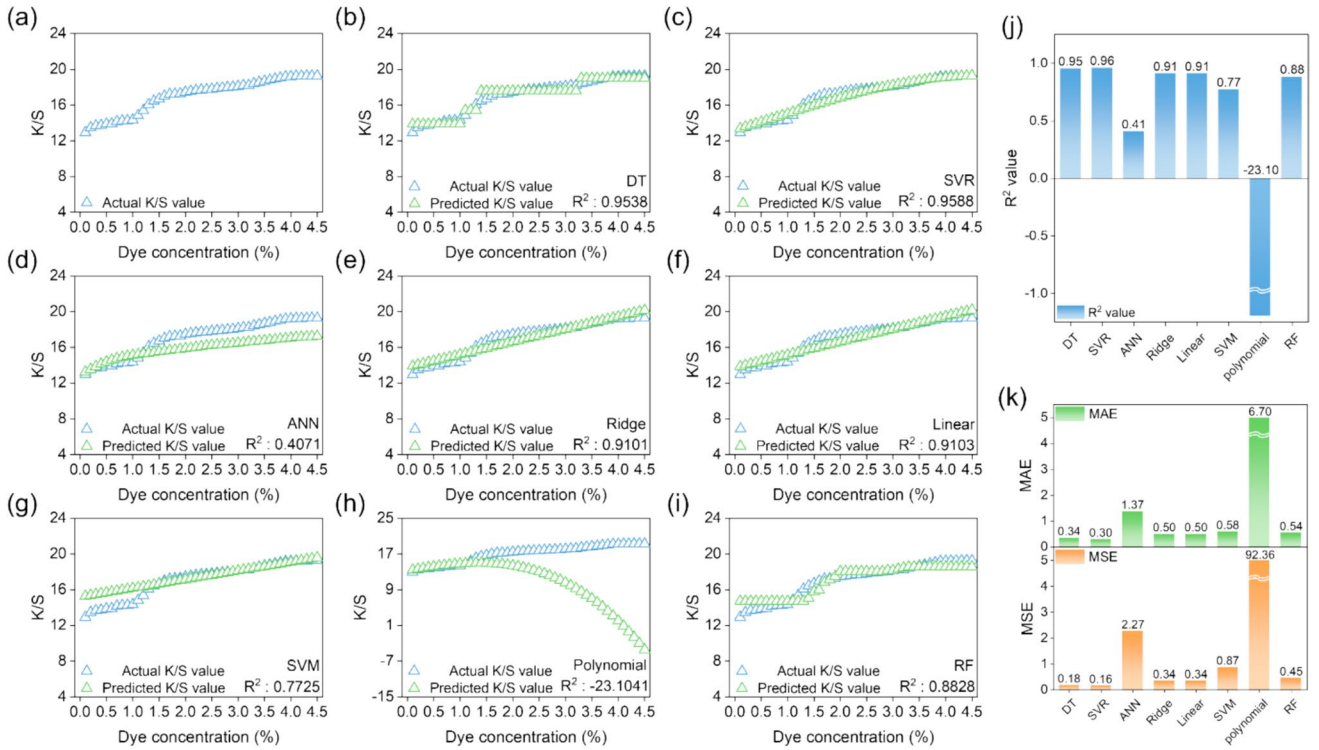

Fig. 3 Predicted K/S curves for dye concentrations 0.1–4.5% owf using various models **a** actual data, **b** DT, **c** SVR, **d** ANN, **e** Ridge regression, **f** Linear regression, **g** SVM, **h** Polynomial regression, **i** RF, and each model performance metrics **j** R^2, and **k** MAE and MSE

across the 0.1–4.5% owf range. These results indicate that SVR effectively captures complex nonlinear relationships and maintains stable predictive performance even under conditions with limited experimental data [55, 56]. As shown in Fig. 3(c), the SVR model successfully reproduced the overall shape of the K/S curve, including the gradual increase with dye concentration, the curvature changes near the saturation point, and the stabilized region beyond saturation. This ability is important in applications where accurately capturing subtle changes around the dye saturation point is essential.

In contrast, the ANN model showed poor performance across all metrics, with an MAE of 1.3663, MSE of 2.2718, and R^2 of 0.4071. This suggests that the ANN may have suffered from overfitting or underfitting due to the relatively small dataset and unnormalized training conditions. Similarly, Polynomial Regression produced highly unstable predictions, with an MAE of 6.7021, MSE of 92.3633, and R^2 of − 23.1041, indicating that overfitting likely occurred as a result of an excessively high polynomial degree. Although the DT, Ridge, and Linear models showed slightly lower performance compared to SVR, their overall prediction curves followed the experimental data reasonably well. However, as shown in the prediction curves in Fig. 3(b), 3(e), and 3(f), these models demonstrated low sensitivity to changes in curve slope, which limited their ability to accurately capture the saturation region. While the RF model produced stable predictions, it failed to capture subtle variations in the curve. Compared to SVR, it showed greater oscillation and irregularity in the predicted values.

As shown by the results, SVR is the most appropriate model for this study, since the goal is not only to ensure regression accuracy but to precisely identify the dye saturation region and determine concentration conditions for achieving deep color expression. Moreover, the results indicate that SVR provides stable generalization performance without requiring extensive parameter tuning, even when the available data are limited, supporting its potential as a data–driven alternative to traditional experiment–based approaches.

3.2 Model Configuration

In this study, SVR was employed to predict the K/S values as a function of dye concentration. SVR is capable of effectively learning the relationship between input and output variables even when the relationship is nonlinear, by using kernel functions [57, 58]. The main idea of SVR is to map input data into a high–dimensional feature space, where linear regression is performed. Rather than explicitly transforming the data, SVR utilizes the kernel trick, which indirectly reflects the high–dimensional representation by

computing inner products through a kernel function [59]. The operation of the kernel function is illustrated in Fig. 4.

In this study, five types of kernel functions were applied, including Linear, Polynomial, RBF (Radial Basis Function), Sigmoid, and Laplacian, to compare their effects on the prediction of K/S values. The corresponding prediction results and the R^2, MAE, and MSE values for each kernel are presented in Fig. 5.

To compare the performance of different kernel types, K/S values were predicted based on dye concentration. As shown in Fig. 5(d) and 5(g), the RBF kernel achieved the best performance, with an MAE of 0.2959, MSE of 0.1579, and R^2 of 0.9588. It accurately reproduced the gradual increase in the curve and the curvature near the saturation point. Consequently, the SVR model was built using the RBF kernel, which demonstrated the highest predictive performance and reliable curve fitting. The RBF kernel is widely used in nonlinear regression tasks and operates by capturing local relationships based on the Euclidean distance between samples [60, 61]. This approach enables effective reproduction of the complex shape of the K/S curve observed in experiments, including changes in slope, curvature near the saturation point, and the gradual transition beyond saturation.

In addition, the SVR model developed in this study was optimized through iterative experiments combined with k-fold cross-validation. Specifically, a fivefold cross-validation scheme was applied solely for hyperparameter tuning within the 0.1–4.5% owf dataset. For each candidate set of parameters C, γ, and ε, the average MAE across the folds was calculated and used to identify the optimal combination. After determining the final hyperparameters, $C = 3.5$, $\gamma = 0.03$, and $\varepsilon = 0.1$, the SVR model was retrained on the entire dataset. The performance metrics reported in Fig. 3(j) and 3(k) therefore represent fits to the training data for the final models trained on all available samples. Here, C controls the penalty strength for errors, γ determines the influence range of the radial basis function (RBF) kernel, and ε defines the tolerance margin for prediction. This combination was found to be the most effective in capturing the gradual slope transitions and the curvature near the saturation point while preventing overfitting (Table S1).

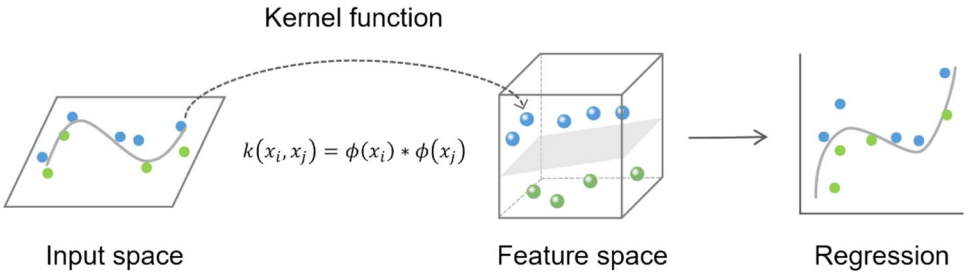

Fig. 4 Schematic illustration of the operational mechanism of the kernel function

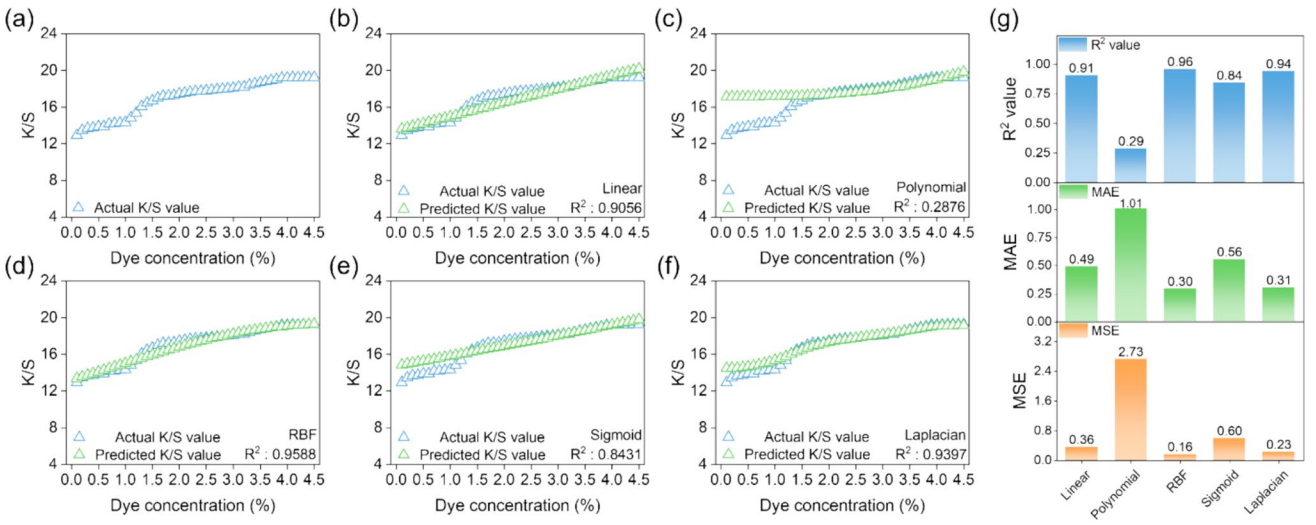

Fig. 5 SVR model prediction results of K/S values for dye concentration 0.1–4.5% owf using different kernel functions **a** actual data, **b** Linear, **c** Polynomial, **d** RBF, **e** Sigmoid, **f** Laplacian, and Kernel function performance metrics **g** R^2, MAE, and MSE

3.3 Prediction of Dye Saturation Point

The SVR–based prediction model was trained on dye concentration data ranging from 0.1–4.5% owf, and extrapolation was then performed for the 4.6–6.0% owf range, which was not included in the training data, in order to estimate the dye saturation region. The prediction results for the extrapolated range (4.6–6.0% owf) obtained using SVR are shown in Fig. 6.

In general, machine learning regression models tend to show reduced predictive stability when applied to inputs outside the training range. However, the SVR model developed in this study extended the shape of the K/S curve in a continuous and smooth manner, generating stable output values even in the extrapolated region. The predicted curve showed a characteristic pattern in which the K/S value increased rapidly at lower dye concentrations, followed by a gradual reduction in slope as the concentration increased, eventually approaching a saturation state. This type of curvature change closely resembles the dye saturation phenomenon observed in actual dyeing processes. It is also consistent with theoretical models, which suggest that once the dye becomes saturated on the fiber surface and within the fiber structure, further increases in dye concentration have little effect on color strength. The saturation region, where the increase in K/S value becomes gradual, is generally determined by factors such as the reaction rate between the dye and the fiber, diffusion resistance within the fiber, and competitive adsorption among dye molecules. The proposed model approximates this complex combination of physical and chemical behaviors in a numerically interpretable form.

According to the model's prediction, the K/S value approached its maximum at approximately 4.9% owf, and beyond this point, the ΔK/S values significantly decreased. Compared to typical MLP–based models or ensemble methods, this result indicates that the SVR model is less sensitive to noise in the training data and has a relatively lower risk of overfitting. It also suggests that SVR is capable of reliably capturing the nonlinear behavior associated with dye saturation, even beyond the trained concentration range.

3.4 Model Performance Validation

As described in the previous section, the SVR–based prediction model was trained on dye concentration data in the range of 0.1–4.5% owf, and extrapolation was performed for the higher concentration range of 4.6–6.0% owf, which was not included in the training data, in order to predict the dye saturation point. According to the model's prediction, the K/S value approached its maximum near 4.9% owf, and beyond this point, the slope of color strength with increasing dye concentration decreased sharply, forming a characteristic saturation curve. To experimentally validate the accuracy of this prediction, fabric samples were dyed at dye concentrations of 5.0, 5.5, and 6.0% owf, which correspond to the extrapolated range predicted by the model, and their K/S values were measured. Figure 7 shows the dye solutions used for dyeing at concentrations of 5.0, 5.5, and 6.0% owf, the residual dye baths after dyeing, and the residual baths after reduction cleaning. Figure 7 also includes the K/S values and surface images of the corresponding dyed fabrics.

As shown in Fig. 7(a), the measured K/S values were 19.36, 19.30, and 19.30 for the 5.0, 5.5, and 6.0% owf dye concentrations, respectively, with a minimal difference of less than 0.06 among the three values. This quantitatively aligns with the model prediction that the change in color strength (ΔK/S) decreases sharply beyond 5% owf, indicating that the SVR model accurately reflects the nonlinear dyeing behavior in the saturation region. In addition, the K/S spectra as a function of wavelength, presented in Fig. 7(b), showed similar spectral shapes and peak intensities across the three samples. This indicates that increasing the dye concentration beyond this point does not lead to further dye uptake. This suggests that the fabric has reached a dye saturation state, meaning that there is little remaining capacity for dye absorption within the fiber. Figure 7(c), 7(d), and 7(e) show images of the dye solution

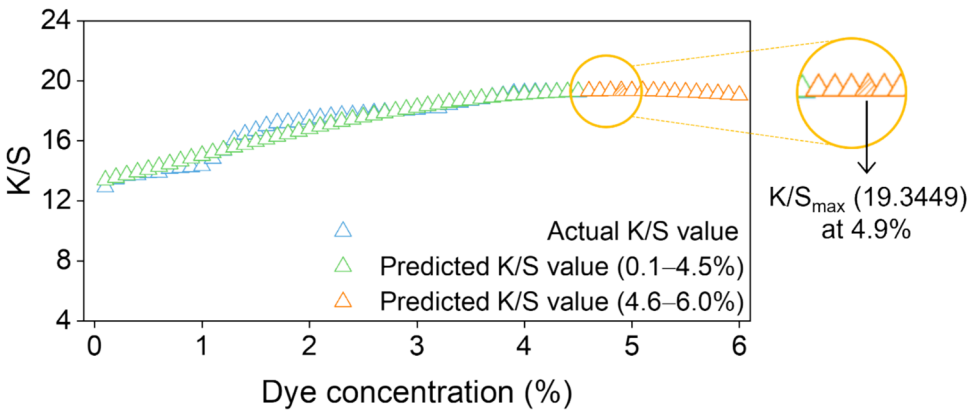

Fig. 6 Predicted K/S values using the SVR model in the extended concentration range of 4.6–6.0% owf

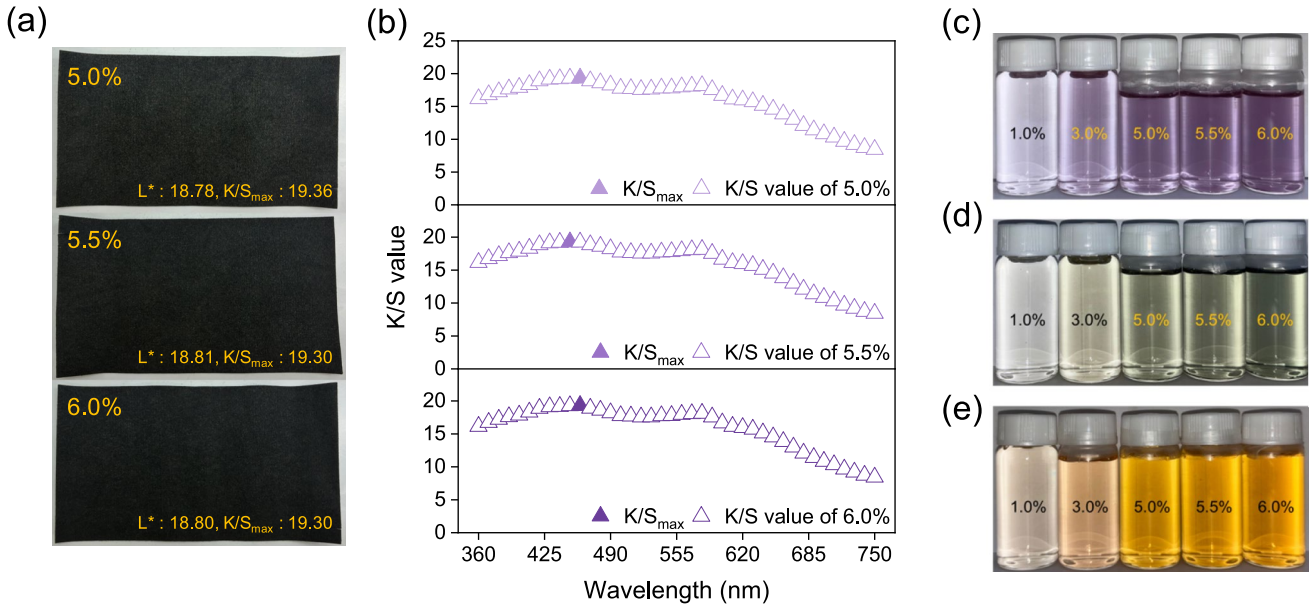

Fig. 7 **a** surface images of dyed fabrics at concentration of 5.0, 5.5, and 6.0% owf, **b** K/S spectra of fabrics dyed at concentration of 5.0, 5.5, and 6.0% owf, **c** 1% diluted solutions of dye baths prepared for fabric dyeing, **d** 10% diluted solutions of residual bath after dyeing, **e** 10% diluted solutions of residual bath after reduction cleaning

before dyeing, the residual bath after dyeing, and the residual bath after reduction cleaning. In the high–concentration samples, the dye bath after dyeing still retained visible color, indicating that the fabric absorbed no further dye at those concentrations. Notably, in samples dyed at 5.0, 5.5, and 6.0% owf concentration, the darker color of the residual bath after reduction cleaning indicates that the fiber had reached saturation and some dye remained unabsorbed. This excess dye did not contribute to any further increase in color strength. This suggests that excessive dye usage does not contribute to further improvement in color strength.

As a result, the SVR–based model developed in this study accurately predicted the saturation trend of the K/S curve even in the extrapolated concentration range. This demonstrates the potential of machine learning models to be utilized in determining optimal dyeing concentrations and establishing resource–efficient strategies in dyeing processes. In addition, by quantitatively predicting the maximum dye uptake concentration, the proposed model enables the determination of an optimal dye concentration that ensures deep shade development without excessive dye use. This contributes to maximizing dye efficiency while minimizing resource consumption in the dyeing process.

4 Conclusion

Eight different regression models were compared, and among them the SVR model with an RBF kernel achieved the highest prediction accuracy ($R^2 \approx 0.96$). In particular, the SVR model effectively approximated the nonlinear saturation curve between dye concentration and K/S value in a smooth and continuous manner and quantitatively identified that saturation of color strength occurs at around 4.9% owf concentration. This is significant in that the optimal dye concentration was determined through data–driven modeling rather than relying on subjective evaluation or repeated experiments. These findings suggest that high predictive accuracy can be achieved even with a limited dataset when an appropriate algorithm is used. In comparison, more complex models were prone to overfitting and showed reduced performance.

To validate the model's extrapolation, fabric samples were dyed at 5.0, 5.5, and 6.0% owf. The measured K/S values closely matched the model's predicted curve, confirming that the SVR model accurately captured the dyeing behavior beyond the training range. Furthermore,

spectral analysis and visual inspection of the dye baths indicated that the fiber had indeed reached saturation, consistent with the model's prediction. This demonstrates that the model can serve as a practical tool for identifying the actual saturation concentration and determining the optimal dye dosage to achieve deep black shade without excessive dye usage.

Such a machine learning–based approach offers various practical applications for dyeing processes. By using the predictive model to establish a threshold for dye concentration, excessive dye consumption can be prevented, which in turn enables a substantial reduction in annual dye usage and wastewater generation. In addition, by modeling the optimal temperature, time, and additive conditions required to achieve the same color strength, it is possible to design energy–efficient and cost–effective dyeing processes. Leveraging existing data also enables rapid simulation and scale–up for new conditions, thereby reducing experimental time and cost. This data–based approach can contribute to the automation and optimization of dyeing processes, serving as a foundation for implementing smart manufacturing systems and developing eco–friendly dyeing technologies, thereby enhancing the sustainability of the textile industry.

Supplementary Information The online version contains supplementary material available at https://doi.org/10.1007/s12221-025-01285-5.

Acknowledgement This research was supported by the Material and Component Development (No. 20024150) funded by Korea Evaluation Institute of Industrial Technology.

Funding Open Access funding enabled and organized by Ulsan National Institute of Science and Technology (UNIST). Korea Evaluation Institute of Industrial Technology, 20024150, Seung Geol Lee

Data Availability The authors confirm that the data supporting the findings of this study are available within the article or its supplementary materials.

Declarations

Conflict of Interest The authors declare that there is no conflict of interest regarding the publication of this article.

References

1. M.M. Islam, A.R. Aidid, J.N. Mohshin, H. Mondal, S. Ganguli, A.K. Chakraborty, Clean. Chem. Eng. **11**, 100165 (2025). https://doi.org/10.1016/j.clce.2025.100165
2. D. Mikucioniene, D. Mínguez-García, M.R. Repon, R. Milašius, G. Priniotakis, I. Chronis, K. Kiskira, R. Hogeboom, R. Belda-Anaya, P. Díaz-García, AUTEX Res. J. **24**, 20240004 (2024). https://doi.org/10.1515/aut-2024-0004
3. A. Azanaw, B. Birlie, B. Teshome, M. Jemberie, Case Stud. Chem. Environ. Eng. **6**, 100230 (2022). https://doi.org/10.1016/j.cscee.2022.100230
4. R. Al-Tohamy, S.S. Ali, F. Li, K.M. Okasha, Y.A.-G. Mahmoud, T. Elsamahy, H. Jiao, Y. Fu, J. Sun, Ecotoxicol. Environ. Saf. **231**, 113160 (2022). https://doi.org/10.1016/j.ecoenv.2021.113160
5. L. Castillo-Suárez, A. Sierra-Sánchez, I. Linares-Hernández, V. Martínez-Miranda, E. Teutli-Sequeira, Int. J. Environ. Sci. Technol. **20**, 10553 (2023). https://doi.org/10.1007/s13762-023-04810-2
6. M.M. Rahman, S. Yoon, S. Choi, S. Kim, Y. Kim, I. Hong, N. Hsan, N. Oh, S. Kumar, J. Koh, Fibers Polym. **26**, 1 (2025). https://doi.org/10.1007/s12221-025-01059-z
7. N.D. Dhage, S.M. Landage, A.R. Mali, Fibers Polym. **26**, 1 (2025). https://doi.org/10.1007/s12221-025-01082-0
8. S. Dutta, S. Adhikary, S. Bhattacharya, D. Roy, S. Chatterjee, A. Chakraborty, D. Banerjee, A. Ganguly, S. Nanda, P. Rajak, J. Environ. Manage. **353**, 120103 (2024). https://doi.org/10.1016/j.jenvman.2024.120103
9. T. Islam, M.R. Repon, T. Islam, Z. Sarwar, M.M. Rahman, Environ. Sci. Pollut. Res. **30**, 9207 (2023). https://doi.org/10.1007/s11356-022-24398-3
10. D. Khandelwal, I. Rana, V. Mishra, K.R. Ranjan, P. Singh, Environ. Res. **261**, 119684 (2024). https://doi.org/10.1016/j.envres.2024.119684
11. M.D. Lord, G. Neve, M. Keating, J. Budhathoki-Uprety, ACS Appl. Polym. Mater. **4**, 6192 (2022). https://doi.org/10.1021/acsapm.2c00959
12. L.M. Biju, V. Pooshana, P.S. Kumar, K.V. Gayathri, S. Ansar, S. Govindaraju, Chemosphere **287**, 132280 (2022). https://doi.org/10.1016/j.chemosphere.2021.132280
13. K. Ramamurthy, P.S. Priya, R. Murugan, J. Arockiaraj, Environ. Sci. Pollut. Res. **31**, 33190 (2024). https://doi.org/10.1007/s11356-024-33444-1
14. A. Dalvand, M. Gholami, A. Joneidi, N.M. Mahmoodi, CLEAN - Soil Air Water **39**, 665 (2011). https://doi.org/10.1002/clen.201000233
15. H.Y. Yen, Desalin. Water Treat. **57**, 10537 (2016). https://doi.org/10.1080/19443994.2015.1039599
16. X. Liu, F. Zhang, S. Liu, Q. Zhao, J. He, J. Wei, X. Dong, J. Clean. Prod. **442**, 141154 (2024). https://doi.org/10.1016/j.jclepro.2024.141154
17. Z. Khatri, M.H. Memon, A. Khatri, A. Tanwari, Ultrason. Sonochem. **18**, 1301 (2011). https://doi.org/10.1016/j.ultsonch.2011.04.001
18. M.L. Goni, N.A. Ganan, R.E. Martini, J. CO2 Util. **54**, 101760 (2021). https://doi.org/10.1016/j.jcou.2021.101760
19. Y. Ma, H. Zheng, T. Cai, F. Zheng, X. Xu, L. Zheng, Cellulose **30**, 11861 (2023). https://doi.org/10.1007/s10570-023-05565-2
20. J. Setthayanond, F. Netzer, K. Seemork, P. Suwanruji, T. Bechtold, T. Pham, A.P. Manian, Cellulose **30**, 4697 (2023). https://doi.org/10.1007/s10570-023-05136-5
21. M.S. Hossain, S.R. Islam, Y. Zhou, A. Khan, H.A. Saeed, Fibers Polym. **26**, 739 (2025). https://doi.org/10.1007/s12221-024-00836-6

22. A. Arroussi, H. Laksaci, M. Djaafri, A. Hiri, O. Khelifi, M. Özacar, B. Ünlü, K. Merabti, M. Bouyoucef, S. Kalloum, Fibers Polym. **26**, 1 (2025). https://doi.org/10.1007/s12221-025-00930-3
23. E.H. Kim, H. Lee, Fibers Polym. **26**, 1 (2025). https://doi.org/10.1007/s12221-025-00892-6
24. L. Villar, M. Pita, B. González, P.B. Sánchez, Fibers Polym. **25**, 2763 (2024). https://doi.org/10.1007/s12221-024-00602-8
25. K. Park, M. Casetta, V. Koncar, Color. Technol. **118**, 319 (2002). https://doi.org/10.1111/j.1478-4408.2002.tb00117.x
26. K. Park, V. Koncar, Color. Technol. **119**, 275 (2003). https://doi.org/10.1111/j.1478-4408.2003.tb00183.x
27. T.A. Elmaaty, M. Sofan, T. Kosbar, H. Elsisi, I. Negm, Fibers Polym. **20**, 2510 (2019). https://doi.org/10.1007/s12221-019-1208-7
28. M.A. El-Rahman, A.Z. Omar, A.R. Kandeel, E.A. Hamed, M.A. El-Atawy, R.M. Keshk, Sci. Rep. **15**, 13410 (2025). https://doi.org/10.1038/s41598-025-96473-x
29. D. Yaseen, M. Scholz, Int. J. Environ. Sci. Technol. **16**, 1193 (2019). https://doi.org/10.1007/s13762-018-2130-z
30. L. Manea, A. Bertea, A. Bertea, IOP Conference Series: Materials Science and Engineering **877**, 012062 (2020). https://doi.org/10.1088/1757-899X/877/1/012062
31. M. Berradi, R. Hsissou, M. Khudhair, M. Assouag, O. Cherkaoui, A. El Bachiri, A. El Harfi, Heliyon **5**, e02711 (2019). https://doi.org/10.1016/j.heliyon.2019.e02711
32. D. Dhruv Patel, S. Bhatt, Biotechnol. Genet. Eng. Rev. **38**, 33 (2022). https://doi.org/10.1080/02648725.2022.2048434
33. M.N. Pervez, W.S. Yeo, L. Lin, X. Xiong, V. Naddeo, Y. Cai, Sci. Rep. **13**, 12363 (2023). https://doi.org/10.1038/s41598-023-39528-1
34. J. Chen, Y. Lin, Y. Liu, Color. Technol. **141**, 223 (2025). https://doi.org/10.1111/cote.12777
35. N. Ingle, W.J. Jasper, Text. Res. J. **95**, 625 (2025). https://doi.org/10.1177/00405175241268619
36. J. Wang, D. Li, H. Tang, X. Li, D. Lei, Appl. Soft Comput. **167**, 112413 (2024). https://doi.org/10.1016/j.asoc.2024.112413
37. Z. Chen, J. Liu, J. Li, M. Yuan, G. Yu, Auton. Intell. Syst. **4**, 19 (2024). https://doi.org/10.1007/s43684-024-00076-8
38. F. Shahmoradi Ghaheh, M. Razbin, M. Tehrani, L. Zolfipour Aghdam Vayghan, M. Sadrjahani, Sci. Rep. **14**, 15067 (2024). https://doi.org/10.1038/s41598-024-64761-7
39. S. Liu, D. Chen, F. Zhang, Q. Zhao, J. He, X. Dong, Dyes Pigments **237**, 112693 (2025). https://doi.org/10.1016/j.dyepig.2025.112693
40. H. Cho, J.E. Lee, A.R. Kim, Y.J. Kang, S.H. Song, J.-H. Sim, S.G. Lee, Fibers Polym. **25**, 3493 (2024). https://doi.org/10.1007/s12221-024-00672-8
41. C. Eyupoglu, S. Eyupoglu, N. Merdan, Z.O. Basyigit, Fibers Polym. **26**, 1 (2025). https://doi.org/10.1007/s12221-025-00936-x
42. Y. Xie, H. Zhang, S. Zhang, S. Xiao, Q. Li, X. Qin, Fibers Polym. **25**, 2985 (2024). https://doi.org/10.1007/s12221-024-00624-2
43. F. Li, C. Chen, Z. Mao, Color. Technol. **138**, 495 (2022). https://doi.org/10.1111/cote.12607
44. J. Zhang, P. Zhang, X. Wu, Z. Zhou, C. Yang, Color. Technol. **133**, 128 (2017). https://doi.org/10.1111/cote.12243
45. A.J. Smola, B. Schölkopf, Stat. Comput. **14**, 199 (2004). https://doi.org/10.1023/B:STCO.0000035301.49549.88
46. P. Rivas-Perea, J. Cota-Ruiz, D.G. Chaparro, J.A.P. Venzor, A.Q. Carreón, J.G. Rosiles, Int. J. Intell. Sci. **3**, 5 (2012). https://doi.org/10.4236/ijis.2013.31002
47. M.S. Zaghloul, R.A. Hamza, O.T. Iorhemen, J.H. Tay, J. Environ. Chem. Eng. **8**, 103742 (2020). https://doi.org/10.1016/j.jece.2020.103742
48. J.C.Y. Ngu, W.S. Yeo, M.K. Chan, J. Nandong, J. Water Process Eng. **64**, 105695 (2024). https://doi.org/10.1016/j.jwpe.2024.105695
49. M.N. Pervez, W.S. Yeo, F. Shafiq, M.M. Jilani, Z. Sarwar, M. Riza, L. Lin, X. Xiong, V. Naddeo, Y. Cai, Heliyon **9**, e12883 (2023). https://doi.org/10.1016/j.heliyon.2023.e12883
50. R. Ribeiro, A. Pilastri, C. Moura, J. Morgado, P. Cortez, Neural Comput. Appl. **35**, 17375 (2023). https://doi.org/10.1007/s00521-023-08596-9
51. T.O. Hodson, Geoscientific Model Dev. (2022). https://doi.org/10.5194/gmd-15-5481-2022
52. T. Chai, R.R. Draxler, Geosci. Model Dev. **7**, 1247 (2014). https://doi.org/10.5194/gmd-7-1247-2014
53. W.P. van de Ven, R.C. van Kleef, Eur. J. Health Econ. **26**, 1 (2024). https://doi.org/10.1007/s10198-024-01709-8
54. D.L. Alexander, A. Tropsha, D.A. Winkler, J. Chem. Inf. Model. **55**, 1316 (2015). https://doi.org/10.1021/acs.jcim.5b00206
55. M. Sabzekar, S.M.H. Hasheminejad, Chaos Solitons Fractals **144**, 110738 (2021). https://doi.org/10.1016/j.chaos.2021.110738
56. W. Liu, S. Lin, X. Li, W. Li, H. Deng, H. Fang, W. Li, J. Environ. Manage. **357**, 120777 (2024). https://doi.org/10.1016/j.jenvman.2024.120777
57. J. Wei, X. He, Measurement and Control **56**, 1705 (2023). https://doi.org/10.1177/00202940231180620
58. B. Üstün, W. Melssen, L. Buydens, Anal. Chim. Acta **595**, 299 (2007). https://doi.org/10.1016/j.aca.2007.03.023
59. C.-H. Ho, C.-J. Lin, J. Mach. Learn. Res. **13**, 3323 (2012)
60. H. Azimi, H. Bonakdari, I. Ebtehaj, Appl Water Sci **9**, 1 (2019). https://doi.org/10.1007/s13201-019-0961-5
61. J. Li, S. Sun, L. Xie, C. Zhu, D. He, Sci. Rep. **14**, 16892 (2024). https://doi.org/10.1038/s41598-024-67197-1